Part 5

Wind derivatives and terminal fall velocities retrieval from "purls" flight patterns in IOP 12

by
Georges Scialom,
Alain Protat,
and Yvon Lemaître

Centre d'étude des Environnements Terrestre et Planétaires, CNRS, Vélizy, France.

5.1 On the interest of Dual-Beam Airborne Velocity Azimuth Display

Since the beginning of modern meteorology, and especially of radar meteorology, the description of the dynamical structure and organization of precipitating systems is a problem of crucial interest for many scientists. This interest has been progressively evolving from the large scale and convective scale motions toward the mesoscale motions on the one hand, and to the scale interactions on the second hand. The evolution toward the mesoscale studies is due to the possible importance of the mechanisms acting at this scale in the origin and the organisation of precipitation. As for cyclogenesis itself, two points of views have been put forward in recent years in order to account for the mesoscale organization of precipitations. One calls to an instability mechanism, slantwise moist convection driven by Conditional Symmetric Instability (Bennetts and Hoskins, 1979; Emanuel 1983; Bennetts and Sharp, 1982; Lemaître and Testud, 1988; Lemaître and Scialom, 1991). The other relies on the existence of an "external" forcing, indeed the frontogenetic forcing itself (Fischer and Lalaurette, 1995), that controls, via diabatic effects, the fine structure of ascent zones, and in particular the formation of weakly stable, strongly sheared areas. The mesoscale is also important because it interacts strongly with the larger scale by energy transfer and with the convective scale by humidity transfer. Another example of the importance of the mesoscale and of the scale interaction is the role shown to be played by the stratiform parts of the precipitating systems, e.g. the squall lines, in the maintenance of the system during several hours, and its propagation as long as it encounters environmental conditions of instability.

The feedback between current theory, experiment, and modelization, along with the crucial role of the mesoscale phenomena has impulsed a considerable development of the radar systems which are facilities particularly suited to this scale. While about twenty years ago, some field experiments (e.g. the GATE experiment, Houze and Betts, 1981) implied no Doppler radar, nowadays the major experiments, either devoted to tropical or to midlatitude meteorology, cannot be conceived and designed without these facilities.

An illustration of this feedback is the huge effort made for more than thirty years in the field of radar meteorology, particularly on devices (Doppler radars), and on analyses allowing the retrieval of the wind field. Concerning the devices, the most original part of the effort was devoted to developing airborne Doppler radars, while the activity on ground-based radars mainly consisted in setting up radar networks, like the NEXRAD network presently deployed over the USA (Alberty et al, 1991). Indeed, for more than ten years, airborne Doppler radars have proved to be an essential step in the evolution of radar meteorology, because of their ability to follow precipitating systems where they are, especially over oceans (Jorgensen et al, 1983; Hildebrand and Mueller, 1985). The first airborne Doppler radars possessed a single antenna scanning planes perpendicular to the aircraft track, offering a single view of the precipitating system. A second view is needed, in order to obtain (by using the mass conservation, or continuity equation) the three-dimensional wind field. Thus, if the aircraft performs successive perpendicular tracks around the precipitating area, the two angles of view allow to obtain the 3D wind field assuming stationarity of the observed system for the considered analyzed data set. Thus in this case, only large scale structure can be described adequately since smaller scale structures are not resolved.

When smaller scale motions are aimed at, two simultaneous scannings are required. This is why the FAST scanning was proposed by Frush et al (1986), and why dual-beam antennas were developed, scanning respectively cones with axis along the aircraft track and having an angle fore and aft with respect to the perpendicular to the track. This was the second step in the improvement of the airborne Doppler radar. The French-US ELDORA-ASTRAIA (Electra Doppler RAdar-Analyse Stéréoscopique par Radar à Impulsion Aéroporté) facility was the first radar of this type. While the ELDORA-ASTRAIA project was going on, the P3-43 radar of the NOAA was equipped with a French dual-beam antenna similar to that of ELDORA-ASTRAIA (Hildebrand and Moore, 1990). Several experiments were conducted which involved one or both of these radars. The CaPE experiment was the first in which the dual-beam antenna, newly installed on the P3-43 radar was operated within squall lines over Florida during summer 1991.

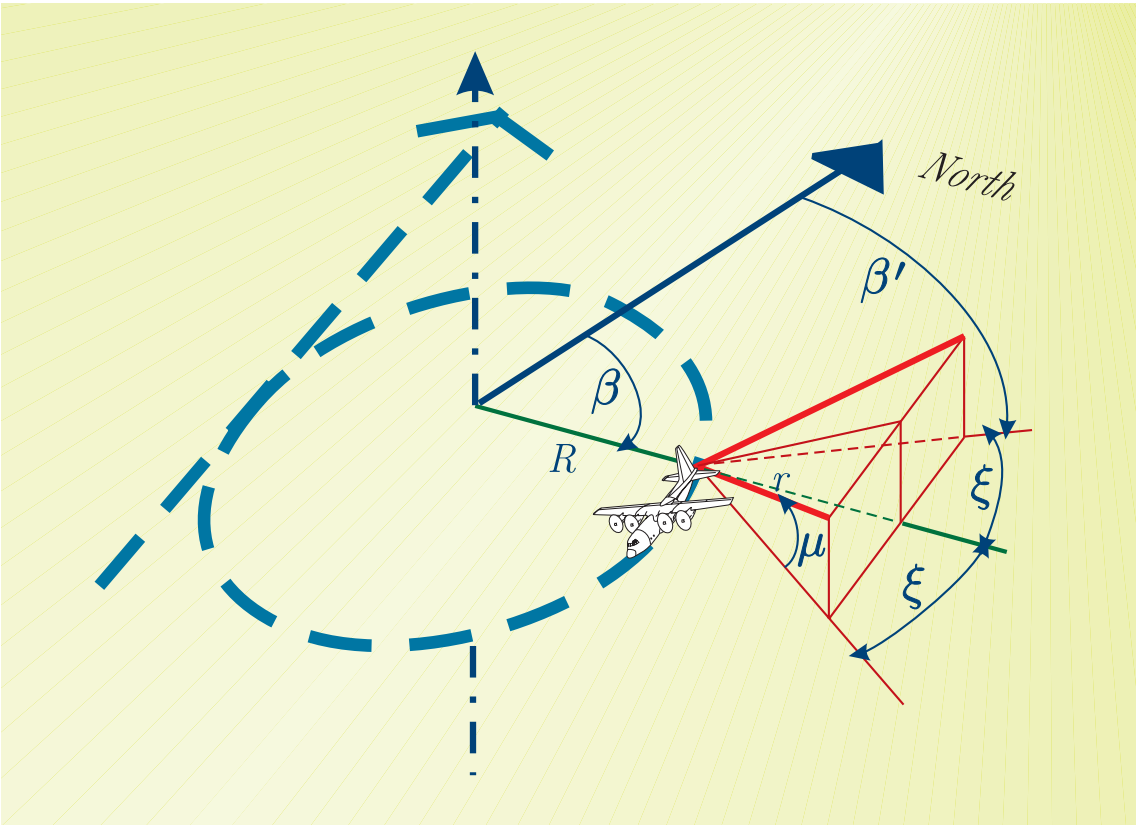

Figure 5.1: *Schematic view of the relevant elevation angles of the dual beam Doppler radar and as well as the azimuth angles.*

From then on, this radar is regularly used to scan tropical cyclones in the Caribbean area. Along with ELDORA-ASTRAIA, both radars were used during the TOGA--COARE experiment (1992-1993). While a lot of analyses are available for the wind field retrieval from ground-based radar data, the various case studies accumulated during the pioneer airborne radar experiments had evidenced the lack of analyses devoted to the wind field retrieval.

Thus, new wind analyses at several scales were developed and tested on the data sets extracted from these experiments. In particular, the cartesian method (Chong

and Campos, 1996), the COPLANE method (Chong and Testud, 1996), and the MANDOP method (Dou et al, 1996), currently used for ground-based radars, were adapted to airborne Doppler radar data. As for the classical (ground-based) VAD analysis which relies upon conical scannings, it can be adapted to airborne radars performing "purls", i.e. circles, in order to provide the mesoscale environmental wind field. When the radar is single-beam, the principle of the adaptation is straightforward but many specific problems must be resolved, as pointed out by Protat et al (1997) who implemented it under the name of SAVAD analysis, and applied it to the data of TOGA-COARE. If the airborne Doppler radar is dual-beam, we show in the following that it is possible to retrieve from the data gathered during the purls the linear approximation of the 3D wind field and the associated physical parameters of crucial importance, such as the vertical vorticity. This approach is called the DAVAD (Dual-beam Airborne Velocity Azimuth Display) analysis.

Developing such new analyses devoted to the retrieval of the wind field at the mesoscale was of crucial importance in view of the international field experiment FASTEX (Fronts and Atlantic Storm Tracks Experiment) which was held on january-february 1997. This experiment was aimed at studying the frontal waves and the cyclogenesis in the Atlantic Ocean. For this objective, frontal systems had to be scrutinized at several scales using in particular the above-noticed two aircraft with their dual-beam antennas. Performing purls all along the experiment allows obtaining the mesoscale wind field and fields of related parameters (vertical vorticity, divergence, deformation, terminal fall velocity of the hydrometeors), in the environment in a very regular way. This strategy of inserting purls along straight line tracks was systematically followed during FASTEX. Moreover, parallel to the development of new instrumentation, considerable efforts have been made on modelling. The design of FASTEX has taken into account the recent merging of both approaches, experimental and by modelling.

In this context, it was decided to include in the Data Base (described in Part 4 of this report) the vertical profiles of the wind and related parameters previously mentioned obtained throughout each sampled system in view of the validation and initialization of models by meteorological fields of experimental origin. Providing the database with the abovementioned parameters will allow to initiate this process.

A very brief and rough summary of the principle of the DAVAD analysis used in the present part of the Report is given. The potential of the approach is then shown, in sections 5.3 to 5.5, through its application to IOP (Intensive Observation Period) 12. This is the same case study as the one of Part 6, where the fields are reconstructed from the radar signal over a large area: this gives access to the 3-D structures present in the cloud system. A quick-look summary of the case is available in section 3.15 of Part 3, page 112 of this Report.

5.2 Outline of the DAVAD retrieval method

The original VAD analysis has been introduced by Browning and Wexler (1968). It relies on the conical scans that can be obtained from a single ground based Doppler radar. Scialom and Testud (1986) have extended this technique to two ground-based Doppler radars, leading to the more accurate Dual VAD.

The nearest equivalent for an airborne Doppler radar results from the aircraft performing a 360°turn around a fixed point, a pattern called "purl". The fixed point in question plays the role of the radar location in the classical problem.

The major difference results from the fact that the antenna(s) are not scanning in the direction of a radius taken from the center of the circle flown by the aircraft (denoted O), unlike a ground base radar. Airborne antennas are (or is, for single beam antennas) looking at an angle from the radius, denoted ξ (Fig. 5.1). It is nevertheless possible to circumvent this difficulty for both single beam antennas (Protat et al., 1997) and dual beam ones (see the submitted version of the present work, Scialom et al., 1999).

The goal is to obtain, at O, vertical profiles of the wind components ($u(z)$, $v(z)$, $w(z)$) together with the terminal fall velocity $V_f(z)$ of the cloud droplets and the first derivatives of the horizontal wind field about point O which combine into the vorticity $\zeta(z)$, the components of the deformation tensor $D_{eT}(z)$ and $Des(z)$ and the divergence $D(z)$. The terminal fall velocity V_f is an important information on the kind of cloud particle and it is also an important component of the observed signal: it is both useful and necessary to retrieve it in order to access the vertical velocity of the air w and, actually, even the horizontal components of the motion.

The input are measurements of the radial velocities V_r (radial with respect to where the antenna are pointing to, *not* with respect to O) for various elevation angles (with respect to the aircraft flight level) μ and at various distances r from the aircraft. Two sets are available in the case of a dual beam antenna. Measurements are available on each of the circles described by each sampling gate in which signal is received back. There is, however, a significant amount of noise in these raw observations and the whole problem is to limit oneself to that part of the scales that can be retrieved with some certainty. The noise is eliminated by creating redundancy in the available data and adjust to them the largest of the scale theoretically available.

At a given level z and a given radius $R + r$ from O, the observed wind V_r is a function of the azimuth β: this function is expanded into a Fourier series limited to order 2 in β:

$$V_r \;=\; V_0 \;+\; V_{c1}\,\cos\beta \;+\; V_{s1}\,\sin\beta \;+\; V_{c2}\,\cos 2\beta \;+\; V_{s2}\,\sin 2\beta. \qquad (5.1)$$

The raw measurements of V_r are turned into a number of values for the five coefficients V_0, V_{c1}, V_{s1}, V_{c2}, V_{s2}, obtained from a discrete set of radiuses and levels.

Another expansion of V_r can be written, first in terms of the wind conditions at the observed point:

$$V_r \;=\; -\,(u\,\sin\beta\,\cos\mu \;+\; v\,\cos\beta\,\cos\mu) \;+\; W(\beta)\sin\mu, \qquad (5.2)$$

where u and v are the usual horizontal wind components and $W(\beta)$ is the observed vertical component of the motion: the latter is dominated by V_f but also contains the vertical wind component w, generally very small, especially in stratiform clouds.

Finally, the horizontal wind itself is expanded to first order (linearly) with respect to its value at the center of the circle, so that equation 5.2 can be turned into an expansion of V_r as a function of β, but with coefficient explicitely given in terms of the various angles (μ, ξ) and distances (R, r) and the unknowns V_f, ζ, D_{eT}, D_{eS} and D, which, for a given level z are assumed to be constant. The detailed expression are beyond the scope of this short summary: see Scialom *et al.*, 1999. Identifying terms from Equation 5.1 and those from the first order development of 5.2 in terms of the wind derivatives yields the equations to be inverted.

To give an example, the first coefficient reads:

$$V_0 \;=\; V_f\,\sin\mu \;-\; 0.5\,D\,\cos\mu\,(r\cos\mu \;+\; R\cos\xi) \;-\; 0.5R\,\zeta\,\sin\xi\cos\mu.$$

Ground base radars are such that $\xi = 0$, so that the first coefficient V_0 in this case is essentially related to the vertical motion (V_f and D, which, because of continuity, relates directly to w). For an airborne radar, this component now mixes up with vorticity ζ.

As the problem is still, by construction, strongly overdetermined, it is solved by a variational technique that makes the most of the measurements made available by the radar specifications. Provided the radar delivers enough data, the variational technique can take care of the new terms. Again, see Scialom *et al.*, 1999 for details.

5.3 Sampling strategy in IOP 12

The present section is devoted to an application of the DAVAD analysis to real data collected during FASTEX. This case study concerns Low 34 observed during FASTEX IOP 12. This low has been documented by Lemaître et al (1999).

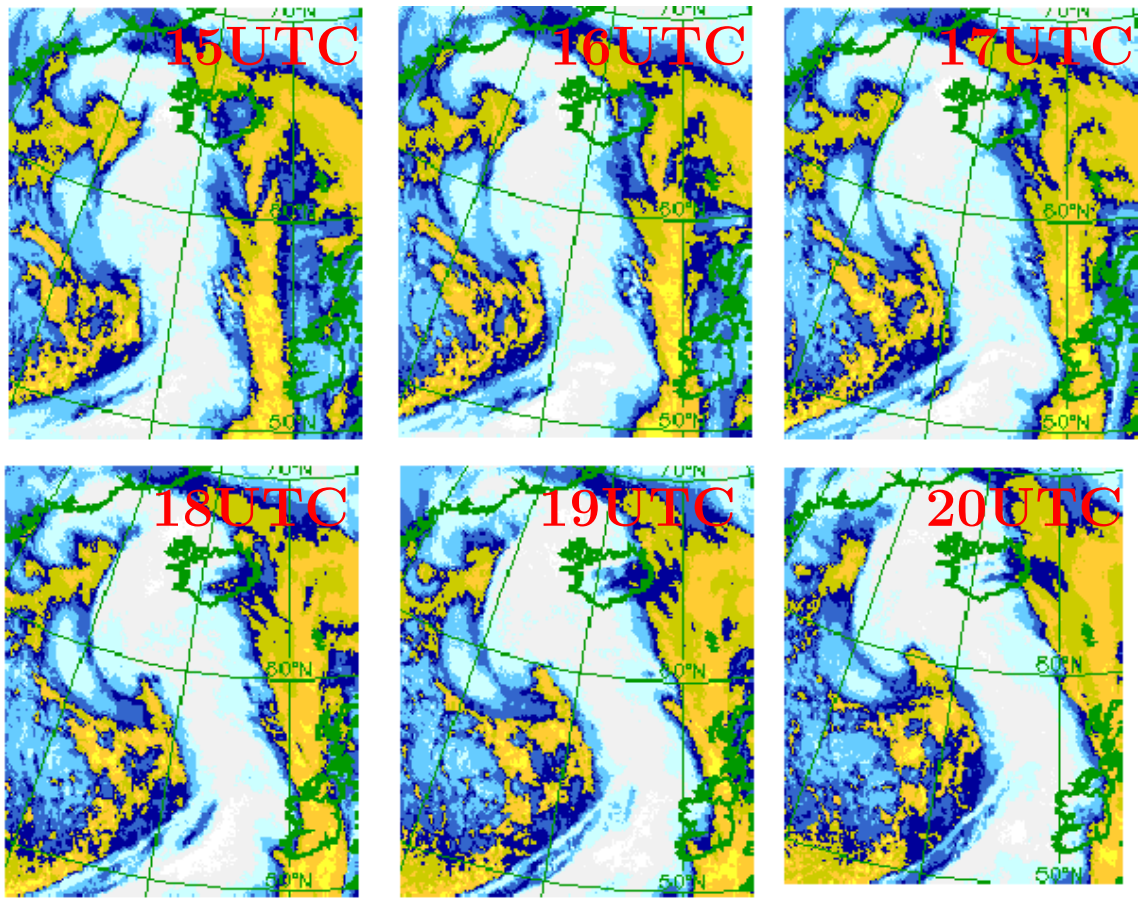

Figure 5.2: *METEOSAT Infra-Red images showing the motion and shape evolution of Low 34 during IOP 12 in the end of its phase of rapid development. Images courtesy of EUMETSAT and the Centre de Météorologie Spatiale of Météo-France.*

The main experimental facilities for that part of the study were the British C130 able to launch dropsondes, the French-US ELDORA-ASTRAIA radar, and the P3-42

NOAA aircraft Doppler radar both equipped with the dual-beam French antenna. The two airborne Doppler radars performed various types of trajectories among which lawnmower-type tracks regularly interrupted by purls (FASTEX Operations Plan, Jorgensen et al, 1996). The lawnmowers allow multiscale description of the lows using the MANDOP analysis (Scialom and Lemaître, 1990, Dou et al, 1996), while purls give mesoscale profiles of the wind and its first derivatives, as shown previously.

The case study which the DAVAD analysis is applied on is the most explosive deepening, roughly −54 mbar in 24 h (Joly et al, 1999) observed during FASTEX (9 february 1997). The METEOSAT satellite IR picture exhibits the evolution of the synoptic situation between 1500 UTC and 2000 UTC, with a drammatic (explosive) formation of Low 34a (as shown by the progressive growth of a cloud head and a dry slot feature that moves northeastward at 40 ms^{-1}, deepens and then tracks toward Iceland (Fig. 5.2). This low was sampled on the northwestern corner of the MSA. The reader is referred to Fig. 6.1 in Part 6, showing the IR picture at 1700 UTC with superimposed the aircraft trajectory in the frame of reference linked to the sampled system. It can be seen that the secondary low has been crossed over and sampled by the aircraft (in the present case, only the P3-42 aircraft was available, the Electra aircraft which bears the ELDORA-ASTRAIA radar being down). This figure illustrates the chosen sampling strategy, "lawnmower" type, which was intended to sample the precipitating systems at several scales and was intensively used during the FASTEX campaign.

The box in Fig. 6.1 delimits the 430×430 km^2 area in which the mesoscale scale retrieval of the dynamics presented in Lemaître et al (1999) was performed using the MANDOP analysis.

Fig. 5.3 exhibits the horizontal cross-section of the 3-D reflectivity field deduced from the P3 tail -radar mesurements, with the aircraft track put in the frame of reference relative to the whole precipitation area. This figure displays the main purls flown by the aircraft along the track between 1500 and 1800 UTC which will be referred to in the rest of this Part.

Lemaître et al (1999), by locating precisely the area covered by the radar within the satellite picture, identified three flows around the secondary low as it can be seen on their cross-section at 0.5 km showing the radar reflectivity and the retrieved wind fields (Fig. 6.4 and 6.5 in Part 6): the Cold Conveyor Belt (CCB) in the northern part of the figure (north of the convective band, with air at intermediate temperature); just south of this flow, the Warm Conveyor Belt (WCB) which wraps around the secondary cyclone. The convective area around the cyclone is the eastern part of the cloud head. The flow in the northwest part is possibly of polar origin, and the one in the southwest part is associated with the dry intrusion. The purls were mostly performed in this radar area as it appears on Fig. 5.3. The wind pattern displayed Fig. 6.5(a) suggests that vorticity on the mesoscale, is cyclonic at flight altitude in the secondary low area. We now summarize the main results from the DAVAD analysis.

5.4 Terminal fall velocity distributions

The vertical profiles of the terminal fall velocity V_f in stratiform or moderately convective areas are generally characterized by values about 5–12 ms^{-1} in the rain, below the 0°C isotherm, and 0–2 ms^{-1}, in the snow, above. In the present case, the processing of purls within stratiform precipitation is given by sample profiles in Fig. 5.4. It shows similar values within error bars. Profiles at 1625, 1634, 1659

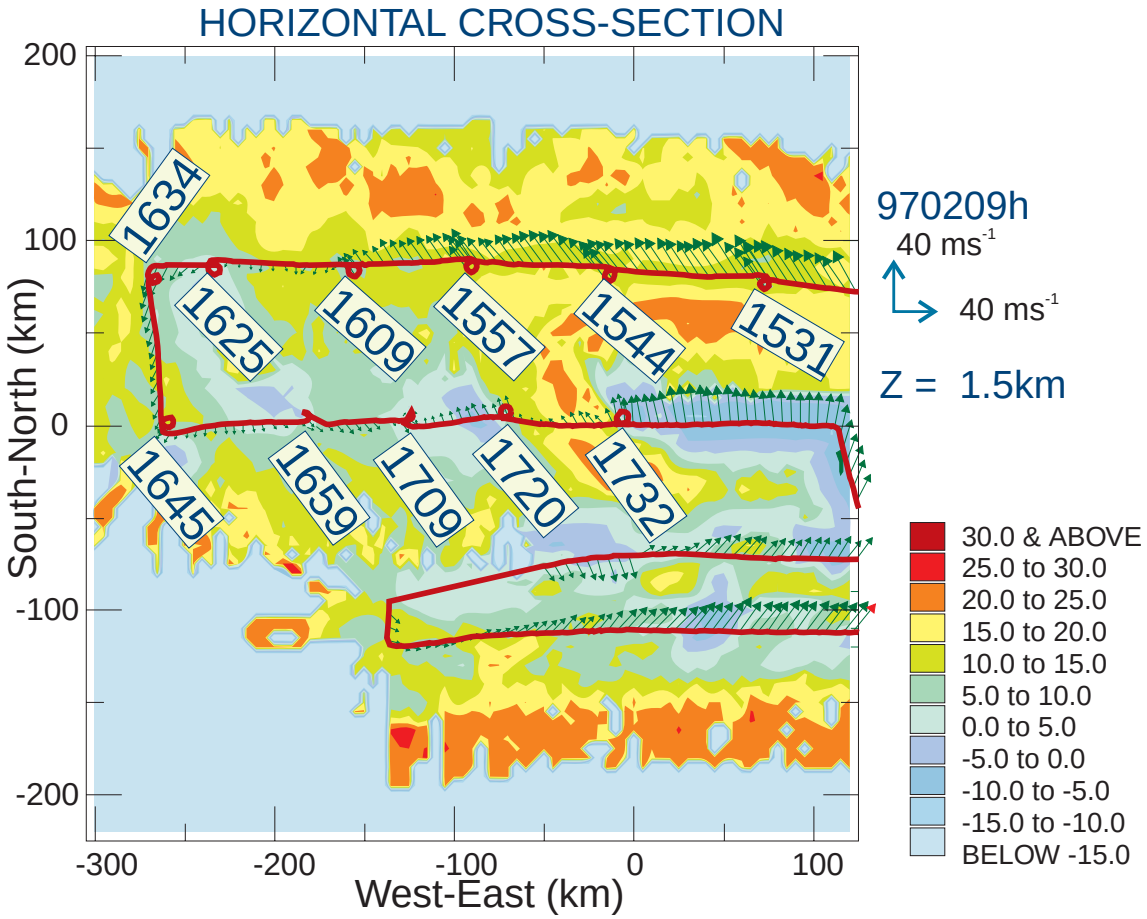

Figure 5.3: *Horizontal cross-section of the 3-D radar reflectivity field deduced from the tail-radar measurements at the flight altitude (1.5 km). The flight track is shown together with the purls labelled by the time at which they have been performed.*

and 1732UTC (not shown), do not exhibit such vertical patterns, which is consistent with the fact these profiles are mainly in nonprecipitating areas (see Fig.5). At last, profiles at 1709 and 1720UTC (also not shown) are intermediate and are obtained in mixed areas.

Fig. 5.5 shows two profiles of reflectivity Z and terminal fall velocity V_f taken in the two main regions of the cyclone, i.e. the CCB area (with overlapping WCB) for the 1531 UTC profile, and the colder northeasterly flow for the 1609 UTC profile; see also Fig. 5.3 for the location of the purls).

The dropsoundings performed by the UK C130 aircraft close to the purls processed to get these profiles show a layer (0°,-10°C layer) located between 1 and 2.5 km altitude, and 0.5 and 2 km for the 1531 and 1609 purls, respectively. This indicates that terminal fall velocity corresponds to ice particles above, and to water below.

We observe that globally, at 1531, the terminal fall velocity is slighly weaker than at 1609. This suggests that precipitating particles are bigger in the CCB area than in the northeasterly flow area. This is consistent with the localization of these purls rather in the high cloud and strong precipitation, for the first one, lower cloud and

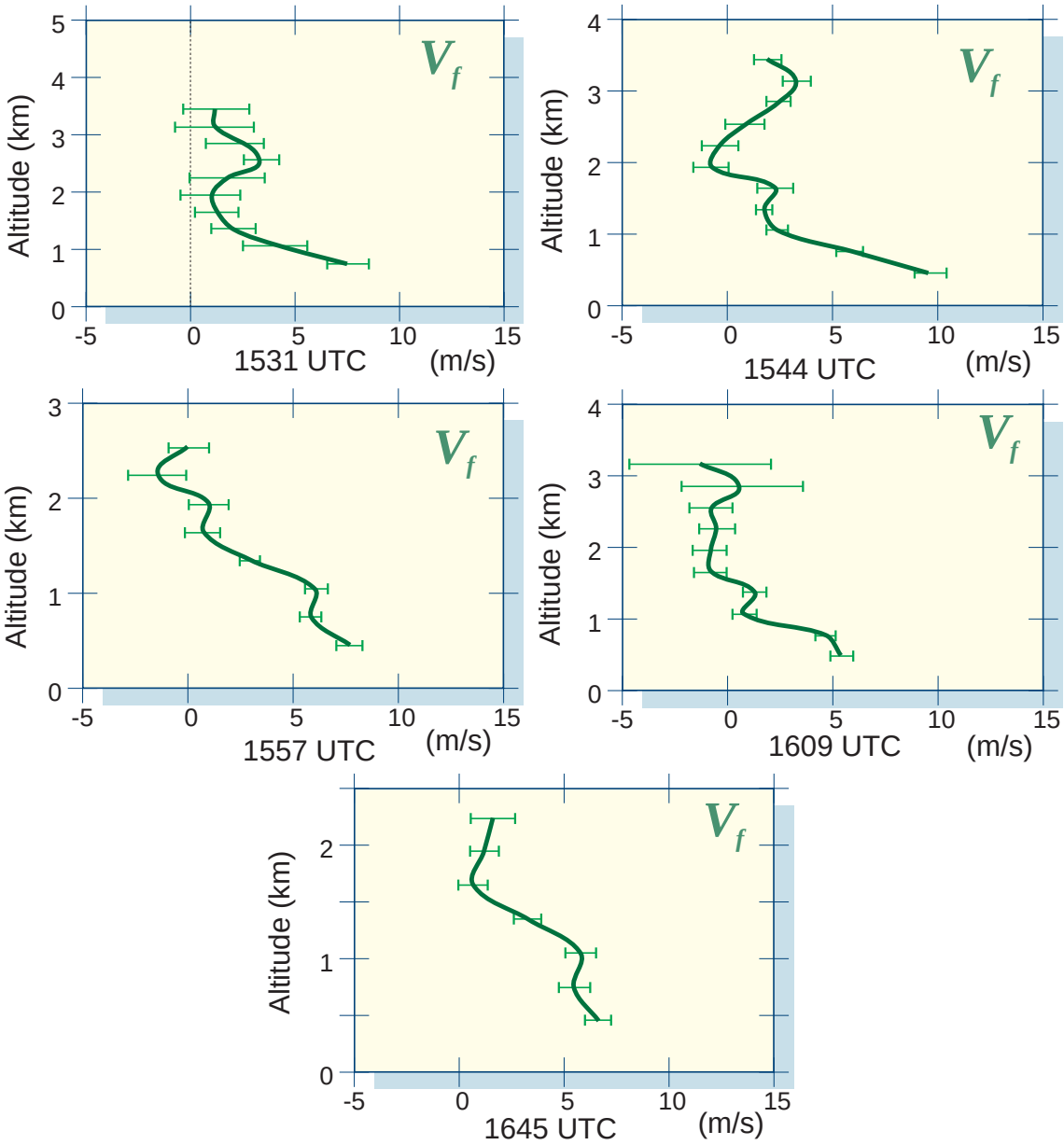

Figure 5.4: *Profiles of the terminal fall velocity V_f obtained for various purls that can be located on Fig. 5.3.*

lighter precipitation for the second. The fall velocity profile exhibits an increase of the fall speed from 0.5 ms^{-1} at 3.5 km to 2.5 ms^{-1} at 2.5 km, which implies that the ice particles tend to become heavier and probably denser. The transition area (0°, −10°C) at 1531 is characterized by a relative decrease in reflectivity and fall velocity, suggesting an evaporation process in that region. Note that the secondary maximum of reflectivity (bright band detected on the radar signal on stratiform precipitation) at 1531 corresponding to the melting layer is located at altitude 750 m. This maxi-

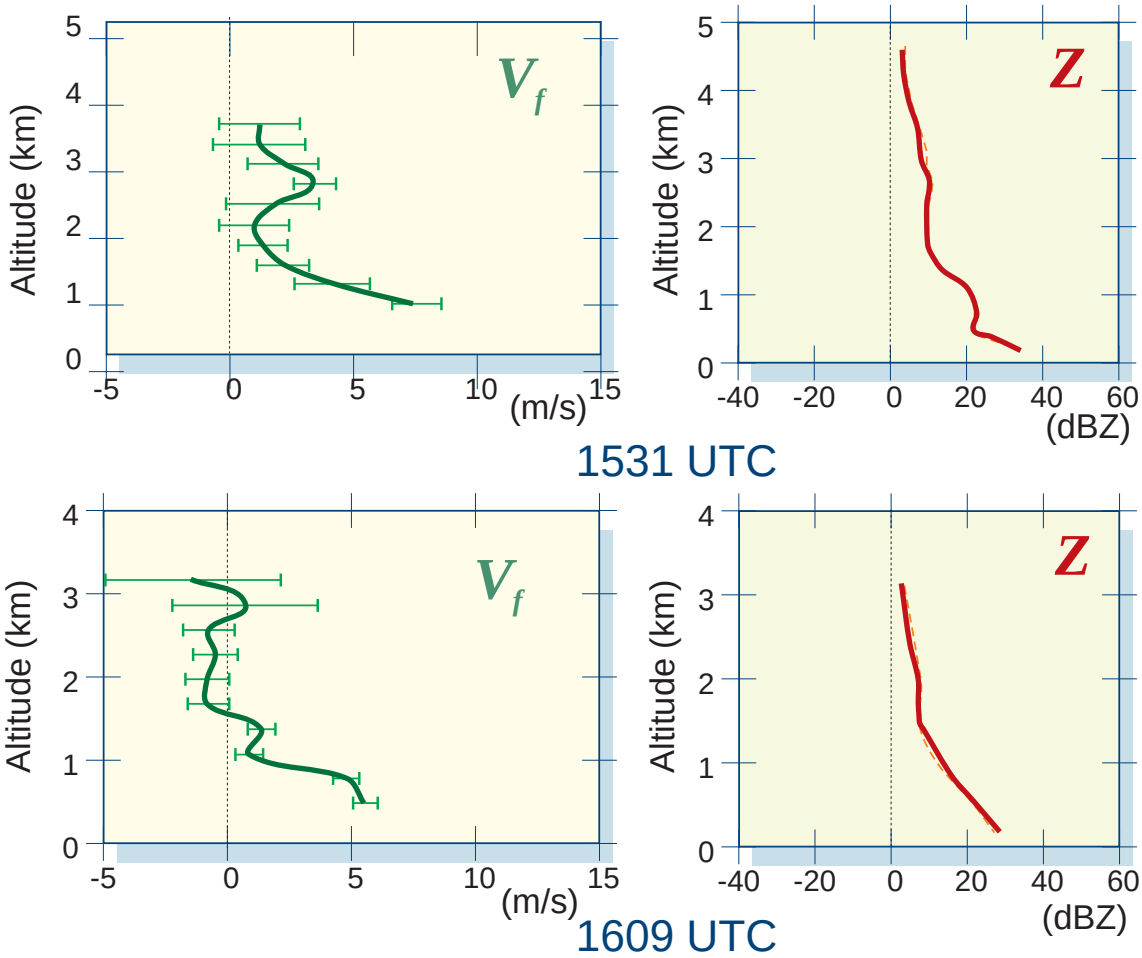

Figure 5.5: *Profiles of the terminal fall velocity V_f together with the corresponding reflectivity Z at two times.*

mum being 300 m below the 0°C isotherm, it means the 0°C isotherm is at 1050 m altitude. The transition between rain and snow on the terminal fall velocity profile, also corresponding to the 0°C isotherm, can be estimated for $V_f = 3.5$ ms^{-1}, i.e. 900 m, in agreement with the previous estimation.

5.5 Wind field properties

The vertical profiles of the wind components u and v (respectively directed eastward and northward as usual) have been retrieved as well for the purls of main interest performed during the aircraft mission (not shown here, see Scialom et al., 1999). They appear strongly variable with time, due to the fact these winds are characteristic of the location of the sampled area with respect to the front. These winds are in good agreement with the winds provided by the wind sensor onboard the aircraft, about 1.5 km in the present case, and also with the vertical profiles obtained about the purls using the MANDOP analysis. However, a slight discrepancy appears between

MANDOP and DAVAD profiles for purls at 1634 and 1645 UTC, due to poor data coverage in the corresponding areas.

Vertical profiles of the vertical component of the vorticity are displayed Fig. 5.6. The vertical vorticity appears to be mainly positive, i.e. cyclonic, consistent with the existence of a low. The profile of 1732 UTC (bottom panel of Fig. 5.6) obtained within the main active part of the low located in the area where the cloud head rolls around the dry slot evidences a maximum at low levels, below 500 m altitude. This is an absolute maximum, as shown by the comparison with another profile located ouside this active area, that of 1609 UTC (top of Fig. 5.6), which exhibits values about twice smaller. This vorticity maximum could be due to the shear between the cloud head and the dry slot area, as suggested by the strong value of the shearing deformation at 1732 UTC (See fig. 5.9 below).

The vertical profiles of the horizontal divergence, of the stretching deformation, and of the shearing deformation also exhibit strong variations according to their location within the system. Comparison with profiles locally determined using the MANDOP analysis shows that the agreement is better within the area far from the edges (1557 and 1720 UTC) than close to the edges (1645, 1659, 1732 UTC and especially 1625, 1634 UTC).

In the main active part of the low, one observes ascending motions in low layers, as shown by the profile of vertical velocity w (Fig. 5.7). Note that outside this active area, for example at 1634 UTC, the vertical velocities are weak, suggesting quasi-horizontal motions in the northwestern part of the cyclone (top of Fig. 5.7). These observations appear consistent with Lemaître et al (1999) results.

The orientation (Browning and Wexler, 1968) of the axis of deformation (or deformation angle) also provides information on the dynamics of the flows (Fig. 5.8). When the angle is null or 90°, that means that pure stretching deformation occurs. For values of 45 or 135°, pure shearing deformation is present. The profile of the deformation angle at 1732 UTC (Right of Figs. 5.8 and bottom of Fig. 5.9) is close to 15°, evidencing that stretching dominates, contrarily to the northwest area for example at 1609 UTC (Left of Fig. 5.8 and top of Fig. 5.9) where shearing dominates (angle close to 45°).

The effect of these deformations on the horizontal temperature gradient can be estimated following Bluestein (1986), expressing the frontogenetic fonction $\mathcal{F}$ in terms

Figure 5.6: *Profiles of the vertical component of vorticity ζ at two particular times. See Fig. 5.3 for locations and Figs. 5.8 and 5.9 for other properties of the horizontal wind field at the same times.*

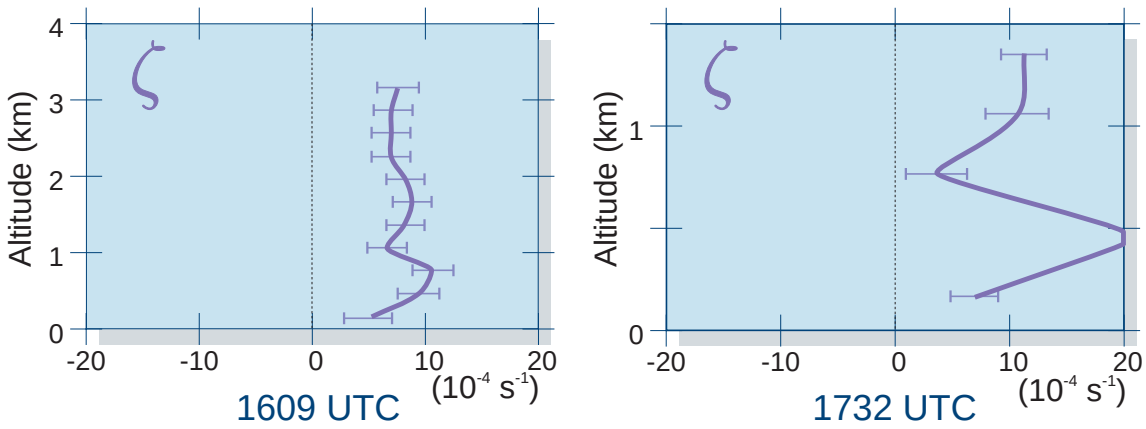

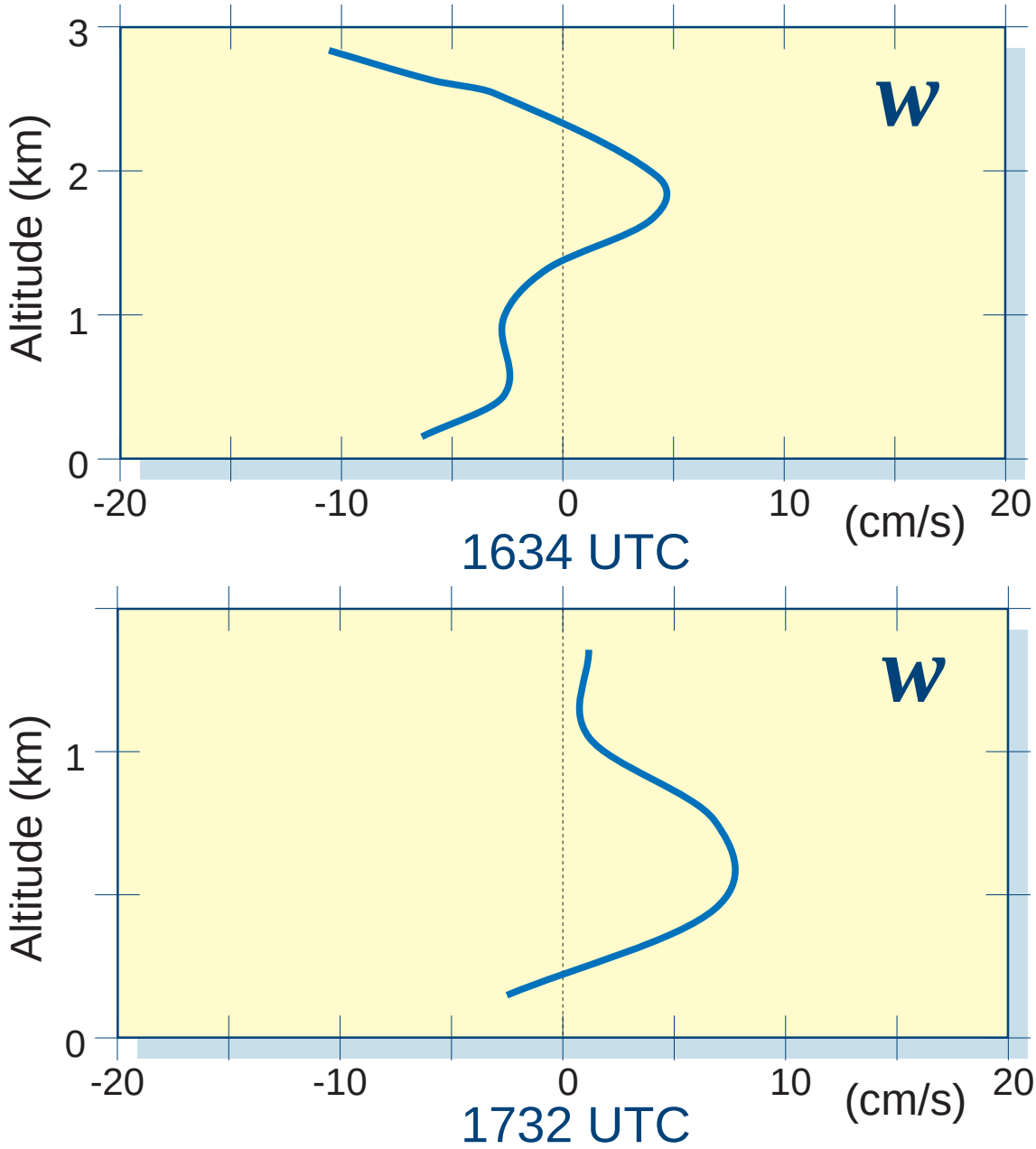

Figure 5.7: *Profiles of the vertical velocity at two particular times. See Fig. 5.3 for locations.*

of these deformations (respectively denoted D_{eT} for its so-called stretching component and D_{eS} for the shearing part) and of divergence D, tilting and diabatic function:

$$\mathcal{F} = \frac{D}{Dt}\|\nabla\theta\| = \frac{1}{2}\left(\frac{\partial S_\theta}{\partial s_\theta} - \frac{\partial\theta}{\partial z}\frac{\partial w}{\partial s_\theta}\right) - \frac{1}{2}\|\nabla\theta\|\,(D - D_{eT}\cos 2\gamma_\theta - D_{eS}\sin 2\gamma_\theta) \tag{5.3}$$

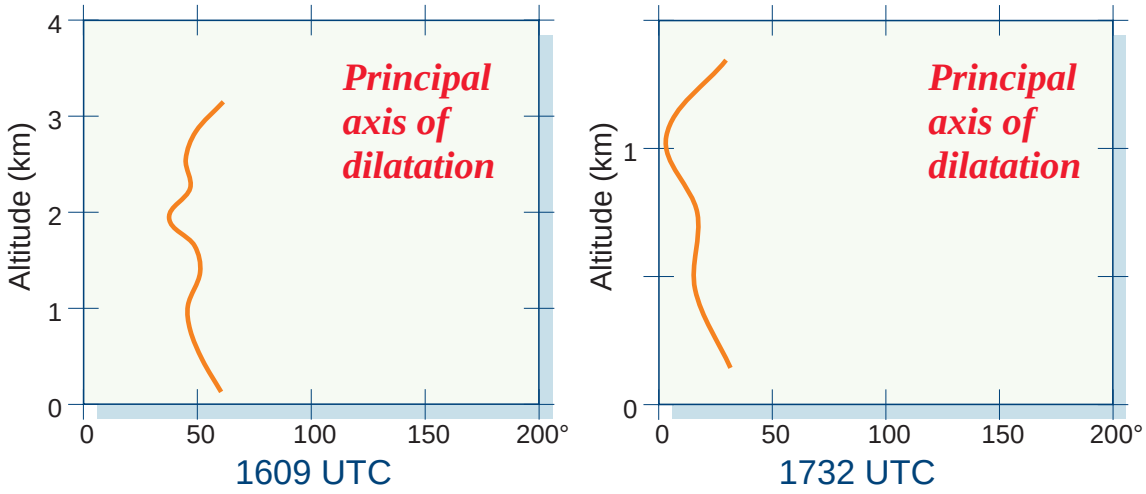

Figure 5.8: *Profiles of the principal axis of dilatation at two particular times. See Fig. 5.3 for locations and Fig. 5.6 and 5.9 for other properties.*

where S_θ is the diabatic heat source of θ, the potential temperature, the coordinate s_θ is taken along the local isentrope (iso-θ), w is the vertical velocity and γ_θ is the angle between the principal axis of dilatation and the local isentrope.

Application of equation 5.3 to the present data leads to the conclusion that, in the active part of the cloud head, the observed stretching deformation is frontolytic (the stretching term of $\mathcal{F}$ is indeed -4×10^{-4} Km^{-1}s^{-1}), and this tends to reduce the horizontal gradient of temperature, whereas on the western part of the cyclone, the observed shearing deformation tends to produce a new baroclinic zone (indeed the shearing term $\mathcal{F}$ is indeed 3×10^{-4} Km^{-1}s^{-1}). These results seem to be consistent with the temperature pattern retrieved by Lemaître et al (1999) who evidence a relatively uniform field on the eastern side of the cloud head, and a well-defined baroclinic region on its western side.

5.6 Concluding remarks

The DAVAD analysis described previously was aimed at retrieving the wind field and its divergence, deformation components and vertical vorticity within the stratiform area of convective precipitating systems. The analysis takes advantage of the VAD approach which it is derived from, since the data are rearranged in the same scanning geometry (conical), and of the two viewing angles under which the dual-beam antenna samples the convective system. This allows all the derivatives to be retrieved, in particular the vertical vorticity.

Simulations reported in Scialom et al. (1999) have shown that the method was able to retrieve the wind and its first derivatives, including the terminal fall velocity of the hydrometeors with good accuracy. Application to real data extracted from the FASTEX experiment data set was possible in spite of the somewhat poor resolution in azimuth of the P3-42 data. The results are highly consistent. The profiles of the fall velocity of the hydrometeors were obtained for all the processed purls. When they are typical of stratiform precipitation areas, they constitute an a posteriori validation for the whole DAVAD analysis and can be included as input for the models. The DAVAD

technique is the best one to access this particular parameter V_f with some precision, and it is subsequently employed as one of the inputs in the 3-D retrieving techniques such as MANDOP: see Part 6.

The wind field is representative of the area in which it is obtained (Warm Conveyor Belt, Cold Conveyor Belt, cold air) in good agreement with the wind sensor onboard the aircraft, and the corresponding derivative terms are also consistent: the vertical vorticity, cyclonic at the mesoscale, is consistent with the one independently obtained by applying the MANDOP analysis on a data set at the scale of the perturbation. The cyclonic vorticity is maximum at the center of the observed secondary low. Identification of the various flows acting about the secondary low are suggested from the divergence, vertical velocity and deformation profiles, depending on the area considered. The paper was aimed at illustrating the capabilities of the proposed analysis of purls. Only a few selected profiles are presented in this paper. However a systematic application of this analysis on all the purls performed during this IOP has been done and will be provided to the FASTEX database.

Figure 5.9: *Profiles of the components of deformation, respectively stretching D_{eT} and shearing D_{eS}, at two particular times. See Fig. 5.3 for locations and previous figures for other properties.*

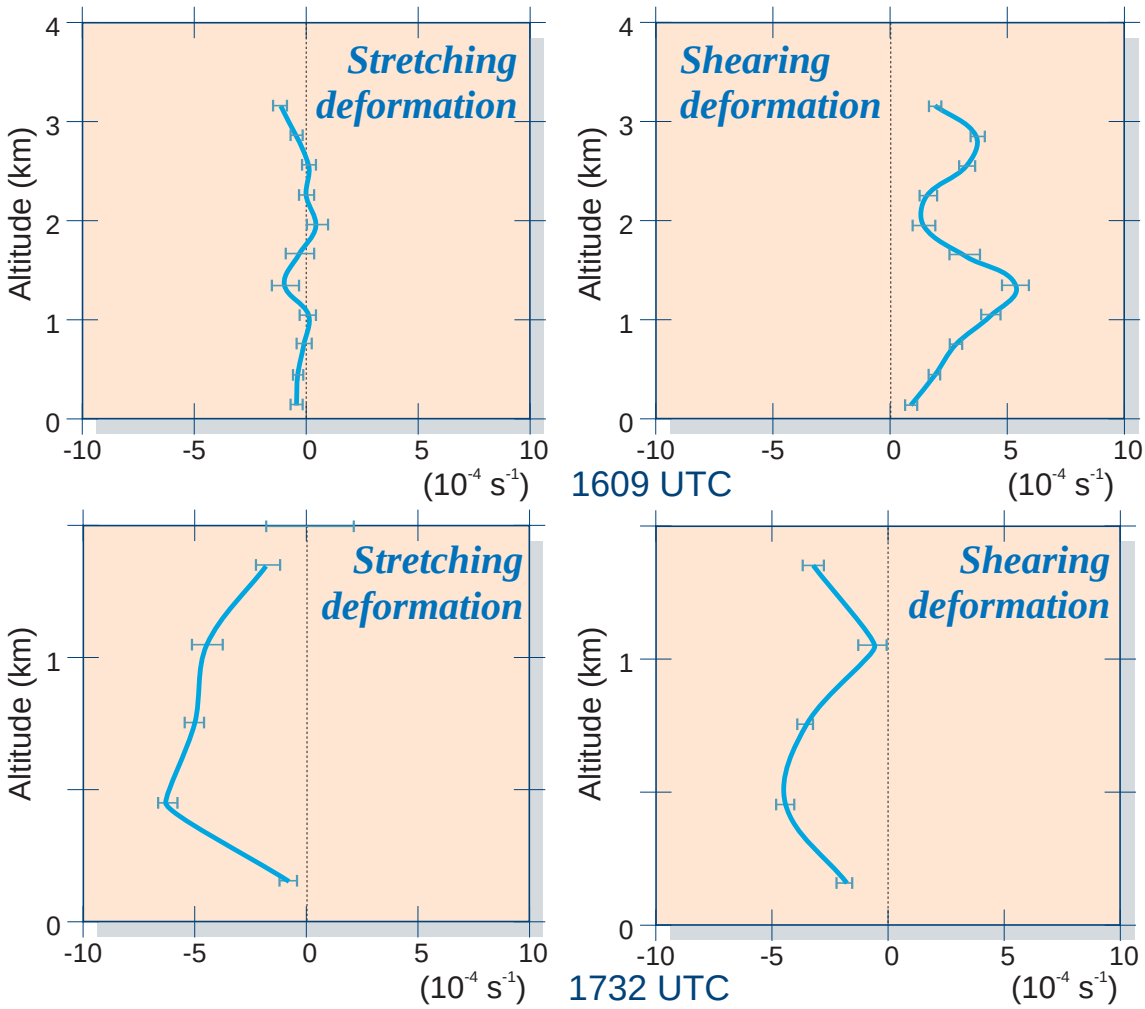

Application to ASTRAIA-ELDORA data set whose resolution is twice better than that of the P3-43 will be also performed for other case studies of the FASTEX experiment.

5.7 References

Alberty, R. L., T. Crum and F. Toepfer, 1991:
The NEXRAD program. Past, present and future. A 1991 perspective.
Preprints, *25th Int. Conf. on Radar Meteorology*, Paris, Amer. Meteor. Soc., 1–8.

Bennetts, D. A. and B. J. Hoskins, 1979:
Conditional symmetric instability: a possible explanation for frontal rainbands.
Quart. J. Roy. Meteor. Soc., **105**, 945–962.

Bennetts, D. A. and J. C. Sharp, 1982:
The relevance of conditional symmetric instability to the prediction of mesoscale frontal rainbands.
Quart. J. Roy. Meteor. Soc., **108**, 595–602.

Browning, K.A., and R. Wexler, 1968:
The determination of kinematic properties of a wind field using Doppler radar.
J. Appl. Meteor., **7**, 105–113.

Bluestein, H. B., 1986:
Fronts and jet streaks: a theoretical perspective.
in *Mesoscale meteorology and forecasting*, American Meteorological Society, Boston, chap. 9, 173–215.

Chong, M. and J. Testud, 1996:
Three-dimensional air circulation in a squall line from airborne dual-beam Doppler radar data: A test of coplane methodology software.
J. Amos. Oceanic. Technol., **13**, 36–53.

Chong, M. and C. Campos, 1996:
Extended overdetermined dual-Doppler formalism in synthesizing airborne Doppler radar data.
J. Amos. Oceanic. Technol., *in press (?!).*

Dou, X. K., G. Scialom, and Y. Lemaître, 1996:
MANDOP analysis and airborne Doppler radar for mesoscale studies.
Quart. J. Roy. Meteor. Soc., **122**, 1231–1261.

Emanuel, K. A., 1983:
On assessing local conditional symmetric instability from atmospheric soundings.
Mon. Weather Rev., **111**, 2016–2033.

Fischer C. and F. Lalaurette, 1995:
Meso-β circulations in realistic fronts. Part II: frontogenetically forced basic states.
Quart. J. Roy. Meteor. Soc., **121**, 1285–1322.

Frush, C. L., P. H. Hildebrand and C. Walther, 1986:
The NCAR airborne Doppler radar. Part II: System design considerations.
Preprints *23rd Radar Meteorology Conf.*, Snowmass, Amer. Meteor. Soc., 151–154.

Hildebrand, P. H., and C. K. Mueller, 1985:
Evaluation of Meteorological airborne Doppler radar. Part I: Dual-Doppler analyses of air motions.
J. Atmos. Oceanic. Technol., **2**, 362–380.

Hildebrand, P.H., and R. K. Moore, 1990:
Meteorological radar observations from mobile platforms.
Chapt 22a in *Radar in Meteorology*, D. Atlas, Ed., Amer. Meteor. Soc., Boston, 287–315.

Houze, R. A. and A. K. Betts, 1981:
Convection in GATE.
Rev. Geophys. Space Phys., **16**, 541–576.

Joly, A., K.A. Browning, P. Bessemoulin, J.P. Cammas, G. Caniaux, J.P. Chalon, S.A. Clough, R. Dirks, K.A. Emanuel, L. Eymard, R. Gall, T.D. Hewson, P.H. Hildebrand, D. Jorgensen, F. Lalaurette, R.H. Langland, Y. Lemaitre, P. Mascart, J.A. Moore, P.O.G. Persson, F. Roux, M.A. Shapiro, C. Snyder, Z. Toth, and R.M. Wakimoto, 1999:
Overview of the field phase of the Fronts and Atlantic Storm-Track Experiment (FASTEX) project.
Quart. J. Roy. Meteor. Soc., **125**, *submitted.*

Jorgensen, D., P. H. Hildebrand and C. L. Frush, 1983:
Feasibility test of an airborne pulse Doppler radar.
J. Climate Appl. Meteor., **22**, 744–757.

Jorgensen D.P., P. Bessemoulin, S. Clough, and J.A. Moore.
Fastex operations plan, 1996.
Technical Report 5, FASTEX Project Office, Centre National de Recherches Météorologiques, 164pp.

Lemaître, Y., and J. Testud, 1988:
Relevance of conditional symmetric instability in the interpretation of wide cold-frontal rainbands.
Quart. J. Roy. Meteor. Soc., **114**, 259–270.

Lemaître, Y. and G. Scialom, 1992:
Three-dimensional mesoscale circulation within a convectivr post-frontal system. Possible role of conditional symmetric instability for triggering convective motions.
Quarterly J. Royal Meteor. Soc., **118 A**, 71–99.

Lemaître, Y., A. Protat and D. Bouniol, 1999:
Pacific and Atlantic "bomb-like" deepening in mature phase: a comparative study.
Quart. J. Roy. Meteor. Soc., *submitted*.

Protat, A., Y. Lemaître, and G. Scialom, 1997:
Retrieval of kinematic fields using a single-beam airborne Doppler radar performing circular trajectories.
J. Atmos. Oceanic Technol., **14**, 769–791.

Scialom, G., and J. Testud, 1986:
Retrieval of horizontal wind field and mesoscale vertical vorticity in stratiform precipitation by conical scannings with two Doppler radars.
J. Atmos. Oceanic Technol., **3**, (4), 693–703.

Scialom, G. and Y. Lemaître, 1990 :
A new analysis for the retrieval of three-dimensional mesoscale wind fields from multiple Doppler radar.
J. Atmos. Oceanic Technol., **7**, 640–665.

Scialom, G., A. Protat, and Y. Lemaître, 1999 :
Vertical structure of a FASTEX secondary cyclone derived from dual-beam airborne radar data.
Quart. J. Roy. Meteor. Soc., *submitted*.

Testud, J., G. Breger, P. Amayenc, M. Chong, B. Nutten and A. Sauvaget, 1980:
A Doppler radar observation of a cold front. Three dimensional air circulation, related precipitation system and associated wave-like motions.
J. Atmos. Sci., **37**, 78–98.